Supporting Information for "Resolving the differences in the simulated and reconstructed temperature response to volcanism"

Feng Zhu[1], Julien Emile-Geay[1], Gregory J. Hakim[2], Jonathan King[3,5], Kevin Anchukaitis[3,4,5]

[1]Department of Earth Sciences, University of Southern California, Los Angeles, CA USA

[2]Department of Atmospheric Sciences, University of Washington, Seattle, WA USA

[3]Department of Geosciences, University of Arizona, Tucson AZ USA

[4]School of Geography and Development, University of Arizona, Tucson AZ USA

[5]Laboratory of Tree-Ring Research, University of Arizona, Tucson AZ USA

Contents of this file

1. Text S1: Settings of the LMR framework

2. Text S2: Reconstructions using the Northern Hemisphere Tree-Ring Network Development (NTREND) network

3. Text S3: Choice of eruption key dates

4. Text S4: Software

————

5. Figure S1: Data from the PAGES 2k network (PAGES 2k Consortium, 2017) assimilated in LMR.

6. Figure S2: Comparison between different LMR implementations, and between model prior and reconstruction.

7. Figure S3: The pseudoproxy experiments (PPEs) that indicate the impact of spatial coverage and seasonality on the correlation between reconstruction and the pseudo-truth.

8. Figure S4: Impact of seasonality on the correlation between reconstruction and the Berkeley Earth instrumental temperature analysis.

9. Figure S5: Correlation between instrumental seasonal temperature observations and real proxy and pseudoproxy composites.

10. Figure S6: The detected signal-to-noise ratio (SNR) in PAGES2k TRW and MXD records.

11. Figure S7: The Northern Hemisphere Tree-Ring Network Development (NTREND) network.

12. Figure S8: The comparison between the model simulated temperature response and the LMR reconstruction assimilating the whole NTREND network.

13. Figure S9: Superposed Epoch Analysis (SEA) of model simulations and LMR reconstructions of the selected 6 eruption events, with individual simulation plotted out.

14. Figure S10: The temperature response to individual eruptions in LMR reconstructions assimilating the whole PAGES 2k Network and GCM simulations, targeting NHMT.

15. Figure S11: The temperature response to individual eruptions in LMR reconstructions assimilating the PAGES 2k MXD Network and GCM simulations, targeting mean summer temperature at proxy locales.

16. Figure S12: The temperature response to individual eruptions in LMR reconstructions assimilating the NTREND MXD Network and GCM simulations, targeting mean summer temperature at proxy locales.

17. Figure S13: Superposed Epoch Analysis (SEA) of model simulations and LMR reconstructions of all eruption events listed in Fig. S10.

18. Figure S14: Superposed Epoch Analysis (SEA) of model simulations and LMR reconstructions using CCSM4 as prior.

19. Figure S15: The comparison of the LMR reconstructions using univariate and bivariate forward operator for TRW records.

20. Figure S16: The available PAGES 2k records with start year earlier than 1257 AD, as well as the age of each of the PAGES 2k record.

21. Table S1: Last millennium model simulations considered in this study.

Introduction

This supporting information provides supplementary figures cited in the main text, as well as detailed information about the real- and pseudo-proxy reconstructions mentioned in the main text. Text S1 details the settings of our LMR experiments. Text S2 describes the reconstruction experiment using the Northern Hemisphere Tree-Ring Network Development (NTREND) (Wilson et al., 2016; Anchukaitis et al., 2017). Text S3 justifies the choice of eruption key dates. Software tools used for the analysis in this study are acknowledged in Text S4.

Text S1: Settings of the LMR framework

The reconstruction experiments in this study follow the general settings:

• Model prior: the isotope-enabled Community Earth System Model (iCESM) simulation (Stevenson et al., 2019; Brady et al., 2019) is used as the model prior. We have also tested using the CCSM4 last millennium simulation (Landrum et al., 2012) as model prior (Fig. S2a, S14) and no significant difference is detected in the temperature response to volcanic eruptions after 1400 AD.

• Ensemble design: 50 Monte Carlo iterations, each using a different randomly chosen 100-member ensemble states from the model prior, and 75% of randomly chosen available proxy records for assimilation (25% for independent verification). This scheme was chosen and explained in Hakim et al. (2016) to balance the needs of accuracy and uncertainty quantification.

- Localization scheme: the Gaspari-Cohn localization function (Gaspari & Cohn, 1999) is used with a radius of 25,000 km (Tardif et al., 2019).

- Forward operator: As in Tardif et al. (2019), we use seasonal bivariate (temperature and moisture) linear regression for tree-ring width (TRW) records, seasonal univariate (temperature) linear regression for maximum latewood density (MXD) records, and annual univariate (temperature) linear regression for all other proxy types as the forward operator in real proxy experiments. The forward operator is calibrated against the Goddard Institute for Space Studies (GISS) Surface Temperature Analysis (GISTEMP) (Hansen et al., 2010) instrumental observation and the gridded precipitation dataset from the Global Precipitation Climatology Centre (GPCC) (Schneider et al., 2014) over the timespan 1850-2015. In pseudoproxy experiments (PPE) the forward operator changes according to the experiment (see main text), and is calibrated against the model's true state over the same interval.

Text S2: Reconstructions using the Northern Hemisphere Tree-Ring Network Development (NTREND) network

The Northern Hemisphere Tree-Ring Network Development (NTREND) (Wilson et al., 2016; Anchukaitis et al., 2017) consists of 54 tree-ring chronologies spanning parts of North America and Eurasia. Of those 54 chronologies, 18 are pure maximum latewood density (MXD), 13 are pure tree-ring width (TRW), and 23 are mixed composites of MXD and TRW. The spatiotemporal sampling is shown in Fig. S7a, S7b.

As a benchmark, we first assimilate the whole NTREND network using the expert-curated seasonality, and the superposed epoch analysis (SEA) shows a similar discrepancy pattern as in IPCC AR5 Fig. 5.8b (Masson-Delmotte et al., 2013) (Fig. S8).

Applying our strategy for gap-bridging described in the main text, we assimilate only the 18 pure MXD records, and reconstruct the boreal summer temperature field, and then perform SEA at proxy locales. The result is shown in Fig. 4b (main text), which shows a better agreement between model simulations and the LMR reconstruction. Note that since 18 records are very few, we assimilate all the records in each ensemble member of assimilation, yield quite narrow uncertainty bands.

Text S3: Choice of eruption key dates Because superposed epoch analysis is an averaging operation, it involves a tradeoff between, on the one hand, maximizing the number of eruption key dates to reduce uncertainties, and on the other hand considerations particular to each eruption.

We chose to exclude eruptions after 1850 because the PMIP3 `past1000` protocol covers only the period (850-1850), and we wanted to be able to compare the greatest number of simulations to reconstructions.

When a cluster of eruptions are close to each other within 10 yrs, we select only the last one to avoid conflating the response of one eruption within the recovery for a preceding event. Note that not all PMIP3 simulations use the same volcanic forcing dataset (Schmidt et al., 2012), and that all differ from the more recent estimates of (Toohey & Sigl, 2017), which is a source of differences between simulations, and between simulations and reconstructions. Also note that neither 1452 nor 1459 (formerly attributed to

the Kuwae caldera) is selected. According to Toohey and Sigl (2017), the 1452 event in Gao, Robock, and Ammann (2008) was misaligned and is actually the 1459 event, so one should select the 1452 event instead of the 1459 event for GCM simulations. However, considering that the 1452 event is close to the 1459 event, we chose to skip both to avoid introducing an obvious discrepancy source for the comparison between GCM simulations and LMR reconstructions. Additionally, the 1761 and 1783 events are also skipped due to issue of misalignment according to Stevenson, Fasullo, Otto-Bliesner, Tomas, and Gao (2017) and Lücke, Hegerl, Schurer, and Wilson (2019).

Text S4: Software

All the analysis in this study was performed in the open-source Python programming language (Van Rossum & Drake Jr, 1995), version 3.7, with the following packages:

- `numpy` (van der Walt et al., 2011)

- `scipy` (Virtanen et al., 2019)

- `pandas` (McKinney, 2010)

- `statsmodels` (Seabold & Perktold, 2010)

- `matplotlib` (Hunter, 2007)

- `seaborn` (Waskom et al., 2018)

All reconstructions were performed with the Last Millennium Reanalysis fast implementation (`LMRt`), of Zhu, Emile-Geay, Hakim, Tardif, and Perkins (2019). This implementation yields nearly identical results compared to the official reconstruction (Fig. S2a), but with additional features:

- Greater flexibility

  – Easy installation

  – Easy importing and usage in Jupyter notebooks

  – Easy setup for different priors, proxies, and Proxy System Models (PSMs)

- Faster speed

  – Much faster PSM calibration due to optimization of algorithm

  – Easy parallel computing with multiprocessing and other techniques

- More modular code structure

References

Anchukaitis, K. J., Wilson, R., Briffa, K. R., Büntgen, U., Cook, E. R., D'Arrigo, R., … Zorita, E. (2017, 5 1). Last millennium Northern Hemisphere summer temperatures from tree rings: Part II, spatially resolved reconstructions. *Quaternary Science Reviews*, *163*, 1–22. doi: 10.1016/j.quascirev.2017.02.020

Brady, E., Stevenson, S., Bailey, D., Liu, Z., Noone, D., Nusbaumer, J., … Zhu, J. (2019). The Connected Isotopic Water Cycle in the Community Earth System Model Version 1. *Journal of Advances in Modeling Earth Systems*, *11*(8), 2547–2566. doi: 10.1029/2019MS001663

Dufresne, J.-L., Foujols, M.-A., Denvil, S., Caubel, A., Marti, O., Aumont, O., … Vuichard, N. (2013, May). Climate change projections using the IPSL-CM5 Earth System Model: from CMIP3 to CMIP5. *Climate Dynamics*, *40*(9-10), 2123–2165. doi: 10.1007/s00382-012-1636-1

Gao, C., Robock, A., & Ammann, C. (2008). Volcanic forcing of climate over the past 1500 years: An improved ice core-based index for climate models. *Journal of Geophysical Research: Atmospheres*, *113*(D23). doi: 10.1029/2008JD010239

Gaspari, G., & Cohn, S. E. (1999). Construction of correlation functions in two and three dimensions. *Quarterly Journal of the Royal Meteorological Society*, *125*(554), 723–757. doi: 10.1002/qj.49712555417

Giorgetta, M. A., Jungclaus, J., Reick, C. H., Legutke, S., Bader, J., Böttinger, M., … Stevens, B. (2013). Climate and carbon cycle changes from 1850 to 2100 in MPI-ESM simulations for the Coupled Model Intercomparison Project phase 5. *Journal of Advances in Modeling Earth Systems*, *5*(3), 572–597. doi: 10.1002/jame.20038

Gordon, C., Cooper, C., Senior, C. A., Banks, H., Gregory, J. M., Johns, T. C., … Wood, R. A. (2000, February). The simulation of SST, sea ice extents and ocean heat transports in a version of the Hadley Centre coupled model without flux adjustments. *Climate Dynamics*, *16*(2-3), 147–168. doi: 10.1007/s003820050010

Hakim, G. J., Emile-Geay, J., Steig, E. J., Noone, D., Anderson, D. M., Tardif, R., … Perkins, W. A. (2016). The last millennium climate reanalysis project: Framework and first results. *Journal of Geophysical Research: Atmospheres*, *121*, 6745 – 6764. doi: 10.1002/2016JD024751

Hansen, J., Ruedy, R., Sato, M., & Lo, K. (2010). Global surface temperature change. *Rev. Geophys.*, *48*, RG4004. doi: 10.1029/2010RG000345

Hunter, J. D. (2007, May). Matplotlib: A 2d Graphics Environment. *Computing in Science Engineering*, *9*(3), 90–95. doi: 10.1109/MCSE.2007.55

Landrum, L., Otto-Bliesner, B. L., Wahl, E. R., Conley, A., Lawrence, P. J., Rosenbloom, N., & Teng, H. (2012, 2014/05/05). Last millennium climate and its variability in ccsm4. *Journal of Climate*, *26*(4), 1085–1111. doi: 10.1175/JCLI-D-11-00326.1

Lücke, L., Hegerl, G., Schurer, A., & Wilson, R. (2019, September). Effects of memory biases on variability of temperature reconstructions. *Journal of Climate.* doi: 10.1175/JCLI-D-19-0184.1

Masson-Delmotte, V., Schulz, M., Abe-Ouchi, A., Beer, J., Ganopolski, A., Rouco, J. G., … Timmermann, A. (2013). Information from Paleoclimate Archives. In T. F. Stocker et al. (Eds.), *Climate Change 2013: The Physical Science Basis. Contribution of Working Group I to the Fifth Assessment Report of the Intergovernmental Panel on Climate Change* (pp. 383–464). Cambridge, United Kingdom and New York, NY, USA: Cambridge University Press. doi: 10.1017/CBO9781107415324.013

McKinney, W. (2010). Data structures for statistical computing in python. In S. van der Walt & J. Millman (Eds.), *Proceedings of the 9th python in science conference* (p. 51 - 56).

Otto-Bliesner, B. L., Brady, E. C., Fasullo, J., Jahn, A., Landrum, L., Stevenson, S., … Strand, G. (2015). Climate variability and change since 850 CE: An ensemble approach with the community earth system model. *Bull. Amer. Meteor. Soc.*, *97*(5), 735–754. doi: 10.1175/BAMS-D-14-00233.1

PAGES 2k Consortium. (2017, 07). A global multiproxy database for temperature reconstructions of the Common Era. *Scientific Data*, *4*, 170088 EP. doi: 10.1038/sdata.2017.88

Rohde, R., Muller, R., Jacobsen, R., Perlmutter, S., Rosenfeld, A., Wurtele, J., … Mosher, S. (2013). Berkeley Earth Temperature Averaging Process. *Geoinformatics & Geostatistics: An Overview*, *2013*. doi: 10.4172/2327-4581.1000103

Rotstayn, L. D., Jeffrey, S. J., Collier, M. A., Dravitzki, S. M., Hirst, A. C., Syktus, J. I., & Wong, K. K. (2012, July). Aerosol- and greenhouse gas-induced changes in summer rainfall and circulation in the Australasian region: a study using single-forcing climate simulations. *Atmos. Chem. Phys.*, *12*(14), 6377–6404. doi: 10.5194/acp-12-6377-2012

Schmidt, G. A., Jungclaus, J. H., Ammann, C. M., Bard, E., Braconnot, P., Crowley, T. J., … Vieira, L. E. A. (2012). Climate forcing reconstructions for use in pmip simulations of the last millennium (v1.1). *Geoscientific Model Development*, *5*(1), 185–191. doi: 10.5194/gmd-5-185-2012

Schmidt, G. A., Ruedy, R., Hansen, J. E., Aleinov, I., Bell, N., Bauer, M., … Yao, M.-S. (2006, January). Present-Day Atmospheric Simulations Using GISS ModelE: Comparison to In Situ, Satellite, and Reanalysis Data. *Journal of Climate*, *19*(2), 153–192. doi: 10.1175/JCLI3612.1

Schneider, U., Becker, A., Finger, P., Meyer-Christoffer, A., Ziese, M., & Rudolf, B. (2014, January). GPCC's new land surface precipitation climatology based on quality-controlled in situ data and its role in quantifying the global water cycle. *Theoretical and Applied Climatology*, *115*(1), 15–40. doi: 10.1007/s00704-013-0860-x

Seabold, S., & Perktold, J. (2010). statsmodels: Econometric and statistical modeling with python. In *9th python in science conference.*

Stevenson, S., Fasullo, J. T., Otto-Bliesner, B. L., Tomas, R. A., & Gao, C. (2017). Role of eruption season in reconciling model and proxy responses to tropical volcanism. *Proceedings of the National Academy of Sciences*, *114*(8), 1822–1826. doi: 10.1073/ pnas.1612505114

Stevenson, S., Otto-Bliesner, B. L., Brady, E. C., Nusbaumer, J., Tabor, C., Tomas, R., … Liu, Z. (2019). Volcanic Eruption Signatures in the Isotope-Enabled Last Millennium Ensemble. *Paleoceanography and Paleoclimatology*, *0*(0). doi: 10.1029/ 2019PA003625

Tardif, R., Hakim, G. J., Perkins, W. A., Horlick, K. A., Erb, M. P., Emile-Geay, J., … Noone, D. (2019, July). Last Millennium Reanalysis with an expanded proxy database and seasonal proxy modeling. *Climate of the Past*, *15*(4), 1251–1273. doi: 10.5194/cp-15-1251-2019

Toohey, M., & Sigl, M. (2017, November). Volcanic stratospheric sulfur injections and aerosol optical depth from 500 BCE to 1900 CE. *Earth System Science Data*, *9*(2), 809–831. doi: 10.5194/essd-9-809-2017

van der Walt, S., Colbert, S. C., & Varoquaux, G. (2011, March). The NumPy Array: A Structure for Efficient Numerical Computation. *Computing in Science Engineering*, *13*(2), 22–30. doi: 10.1109/MCSE.2011.37

Van Rossum, G., & Drake Jr, F. L. (1995). *Python tutorial.* Centrum voor Wiskunde en Informatica Amsterdam, The Netherlands.

Virtanen, P., Gommers, R., Oliphant, T. E., Haberland, M., Reddy, T., Cournapeau, D., … Contributors, S. . . (2019, Jul). SciPy 1.0–Fundamental Algorithms for Scientific

Computing in Python. *arXiv e-prints*, arXiv:1907.10121.

Waskom, M., Botvinnik, O., O'Kane, D., Hobson, P., Ostblom, J., Lukauskas, S., … Qalieh, A. (2018, July). *mwaskom/seaborn: v0.9.0 (july 2018).* Zenodo. doi: 10.5281/zenodo.1313201

Watanabe, S., Hajima, T., Sudo, K., Nagashima, T., Takemura, T., Okajima, H., … Kawamiya, M. (2011, January). MIROC-ESM 2010: Model description and basic results of CMIP5-20c3m experiments. *Geoscientific Model Development*, *4*(4), 845– 872. doi: 10.5194/gmd-4-845-2011

Wilson, R., Anchukaitis, K., Briffa, K. R., Büntgen, U., Cook, E., D'Arrigo, R., … Zorita, E. (2016, 2 15). Last millennium northern hemisphere summer temperatures from tree rings: Part I: The long term context. *Quaternary Science Reviews*, *134*, 1–18. doi: 10.1016/j.quascirev.2015.12.005

Wu, T., Song, L., Li, W., Wang, Z., Zhang, H., Xin, X., … Zhou, M. (2014, February). An overview of BCC climate system model development and application for climate change studies. *Journal of Meteorological Research*, *28*(1), 34–56. doi: 10.1007/ s13351-014-3041-7

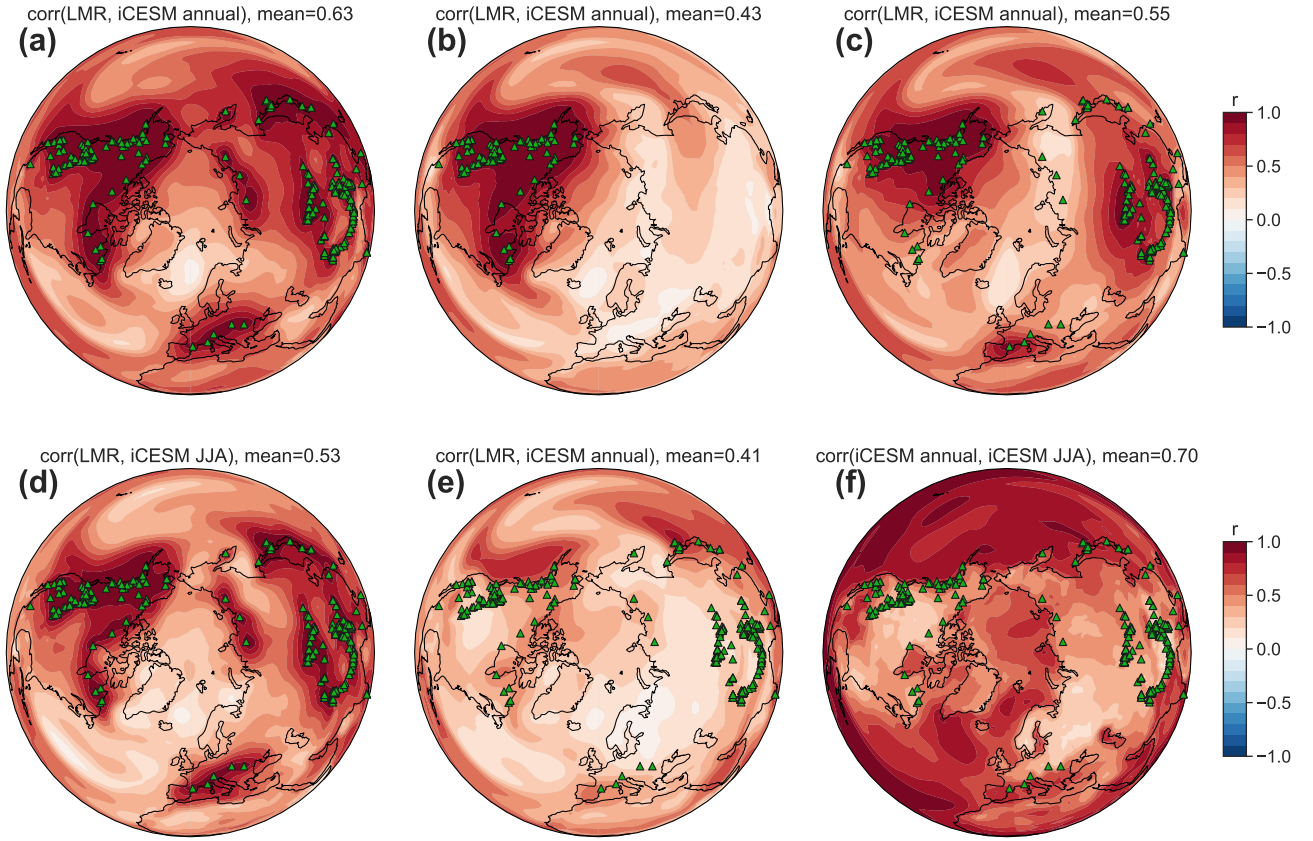Zhu, F., Emile-Geay, J., Hakim, G. J., Tardif, R., & Perkins, A. (2019, December). *LMR Turbo (LMRt): a lightweight implementation of the LMR framework.* Zenodo. doi: 10.5281/zenodo.3590258

(a)

⬠	Bivalve_d18O (n=1)
✚	Corals and Sclerosponges_Rates (n=8)
✖	Corals and Sclerosponges_SrCa (n=25)
⬤	Corals and Sclerosponges_d18O (n=60)
◁	Ice Cores_MeltFeature (n=1)
◇	Ice Cores_d18O (n=31)
▷	Ice Cores_dD (n=7)
◆	Lake Cores_Misc (n=3)
■	Lake Cores_Varve (n=6)
▲	Tree Rings_WidthPages2 (n=347)
▼	Tree Rings_WoodDensity (n=59)

(b)

- Tree Rings_WidthPages2
- Corals and Sclerosponges_d18O
- Tree Rings_WoodDensity
- Ice Cores_d18O
- Corals and Sclerosponges_SrCa
- Corals and Sclerosponges_Rates
- Ice Cores_dD
- Lake Cores_Varve
- Lake Cores_Misc
- Ice Cores_MeltFeature
- Bivalve_d18O

Figure S1.   Data from the PAGES 2k network (PAGES 2k Consortium, 2017) assimilated in LMR. (a) Spatial coverage by archive type. (b) Temporal availability by archive type.
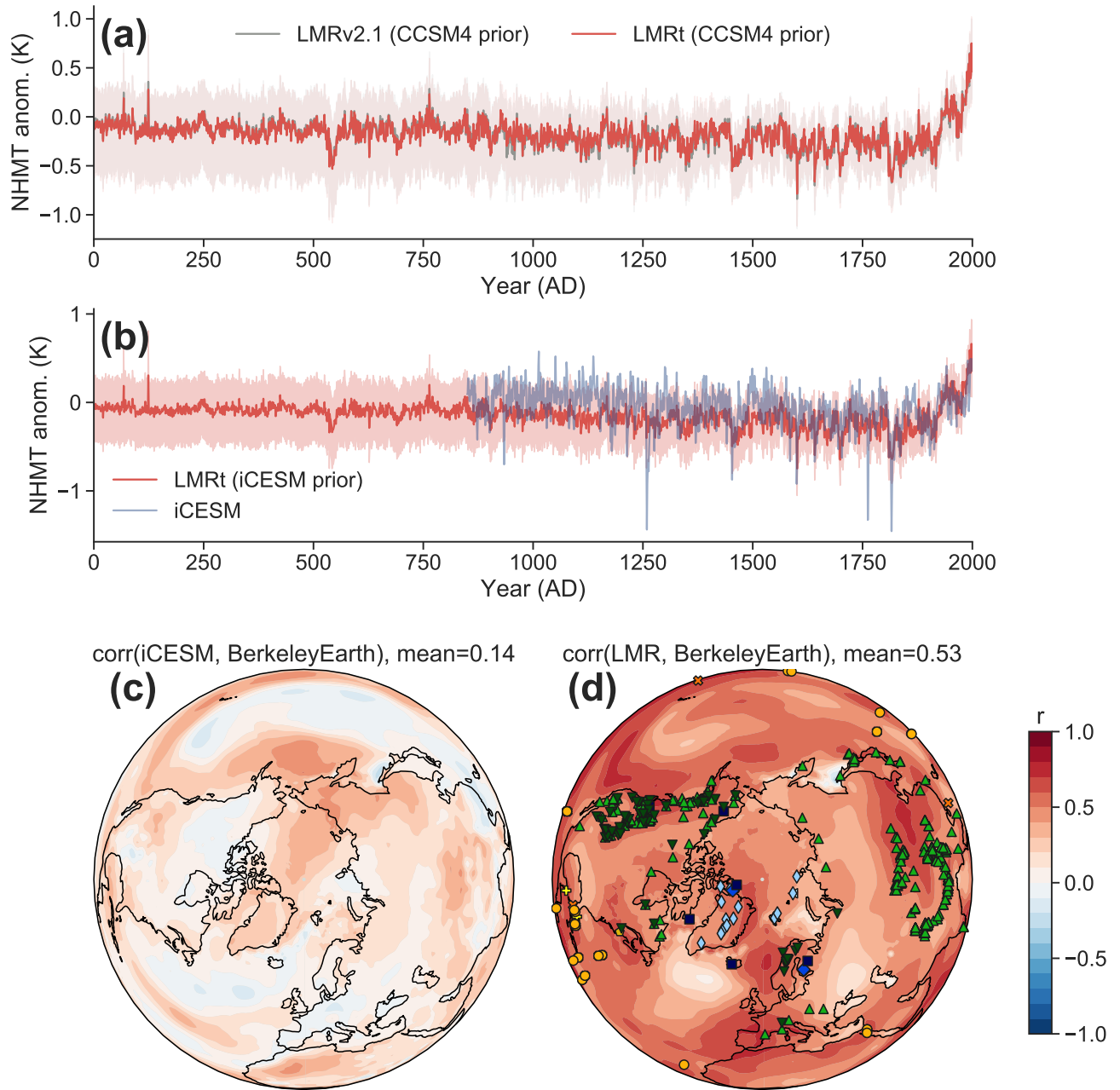
Figure S2. (a) The reconstructed northern hemisphere mean temperature (NHMT) series using the official LMR implementation (Tardif et al., 2019) and the lightweight implementation used in our study `LMRt` (Zhu et al., 2019), using the same CCSM4 model prior (Landrum et al., 2012) and the PAGES 2k phase 2 dataset (PAGES 2k Consortium, 2017). (b) The LMR reconstructed NHMT series assimilating the PAGES 2k network, along with its model prior, the simulated NHMT series from the isotope-enabled Community Earth System Model (iCESM) (Stevenson et al., 2019; Brady et al., 2019). (c) The correlation between the surface temperature simulated by iCESM and the instrumental observation Berkeley Earth instrumental temperature analysis (Rohde et al., 2013) over 1880 to 2000. (d) Same as (b) but for LMR reconstruction assimilating the PAGES 2k network. The symbols follow that in Fig. S1.

corr(LMR, iCESM annual), mean=0.63 **(a)**

corr(LMR, iCESM annual), mean=0.43 **(b)**

corr(LMR, iCESM annual), mean=0.55 **(c)**

corr(LMR, iCESM JJA), mean=0.53 **(d)**

corr(LMR, iCESM annual), mean=0.41 **(e)**

corr(iCESM annual, iCESM JJA), mean=0.70 **(f)**

Figure S3. **The pseudoproxy experiments (PPEs) that indicate the impact of spatial coverage and seasonality on the correlation between reconstruction and the pseudo-truth.** (a) The pseudoproxies are generated as perfect temperature recorders of the annual temperature simulated by iCESM, and the whole network is assimilated. (b) Same as (a), but only 50 records over North America (NA) region are assimilated. (c) Same as (a), but only 50 records over Northern Hemisphere (NH) are assimilated. (d) Same as (a), but the pseudoproxies are generated as perfect temperature recorders of the summer temperature simulated by iCESM, and summer temperature field is reconstructed. (e) Same as (d), but annual temperature field is reconstructed. (f) The correlation between annual temperature and summer temperature simulated by iCESM.

corr(LMR, BerkeleyEarth), mean=0.21 (a)

corr(LMR, BerkeleyEarth), mean=0.22 (b)
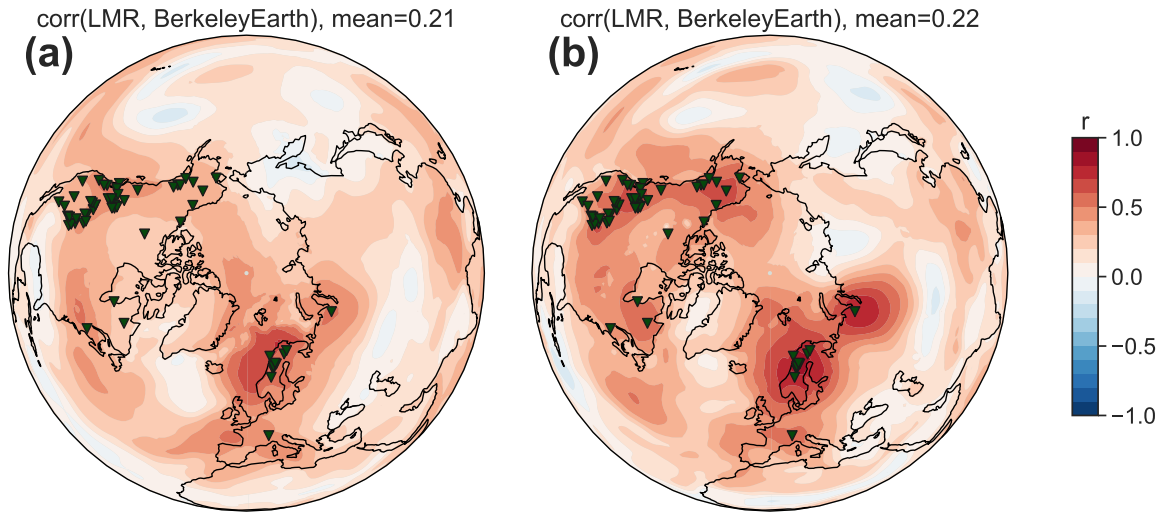
Figure S4. Impact of seasonality on the correlation between the reconstructions assimilating the MXD network and the Berkeley Earth instrumental temperature analysis (Rohde et al., 2013). (a) Reconstructing annual temperature (b) Reconstructing summer temperature. Note that both experiments use real, not pseudo, proxies.

**Table S1.** Last millennium model simulations considered in this study

Model	Experiment ID
iCESM (Stevenson et al., 2019; Brady et al., 2019)	-
CESM1 (Otto-Bliesner et al., 2015)	b.e11.BLMTRC5CN.f19_g16.001
BCC CSM1.1 (Wu et al., 2014)	past1000_r1i1p1
GISS-E2-R (Schmidt et al., 2006)	past1000_r1i1p1
HadCM3 (Gordon et al., 2000)	past1000_r1i1p1
IPSL-CM5A-LR (Dufresne et al., 2013)	past1000_r1i1p1
MIROC-ESM (Watanabe et al., 2011)	past1000_r1i1p1
MPI-ESM-P (Giorgetta et al., 2013)	past1000_r1i1p1
CSIRO (Rotstayn et al., 2012)	past1000_r1i1p1
CCSM4 (Landrum et al., 2012)	past1000_r1i1p1
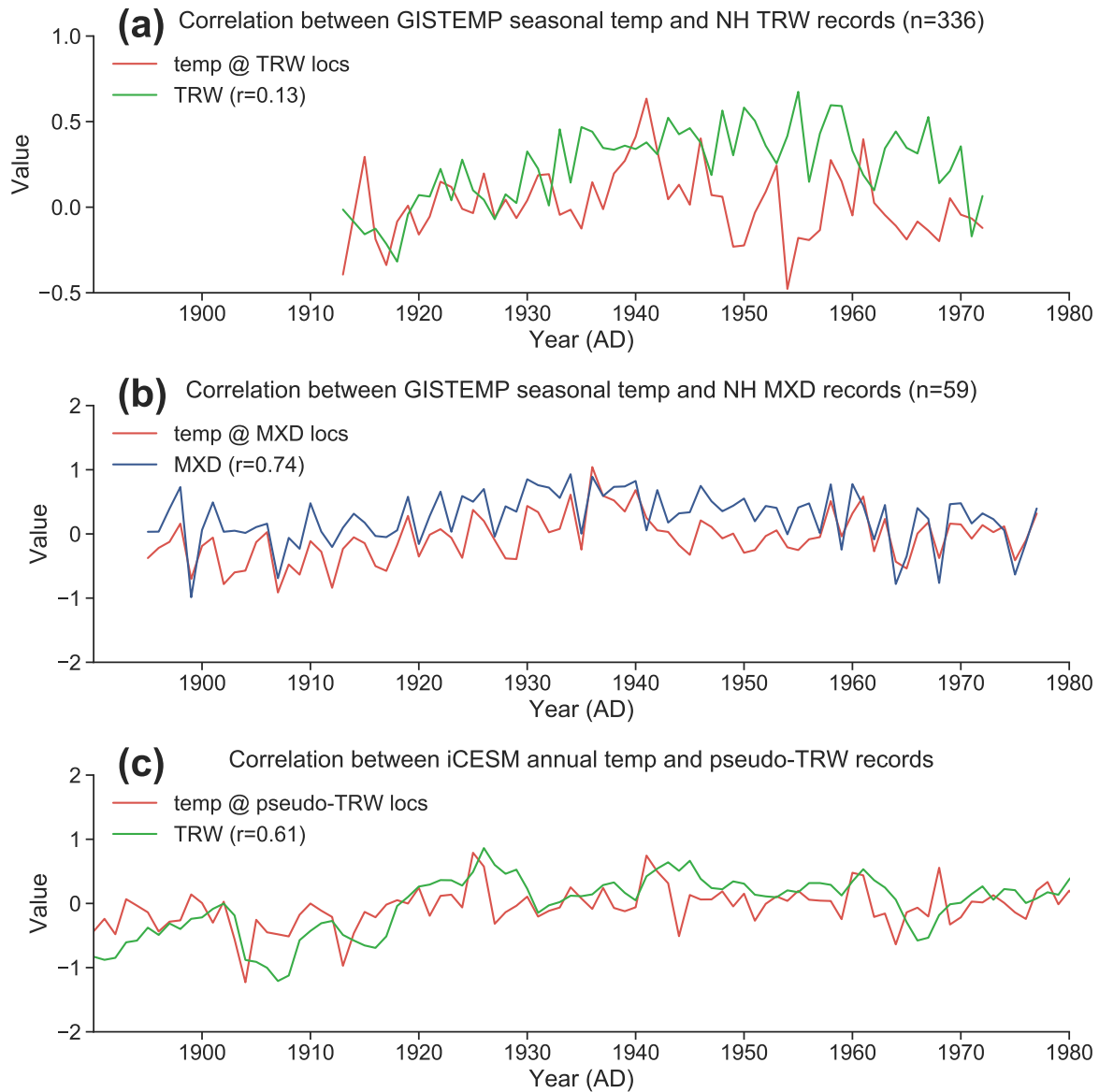
Figure S5. (a) The NH TRW composites compared to the seasonal observational temperature, the Goddard Institute for Space Studies (GISS) Surface Temperature Analysis (GISTEMP) (Hansen et al., 2010), at proxy locales. (b) Same as (a), but for MXD. (c) The composite of the pseudoproxy that is generated as temperature smoother with a 5-yr moving average filter, compared to the iCESM simulated temperature at the proxy locales.
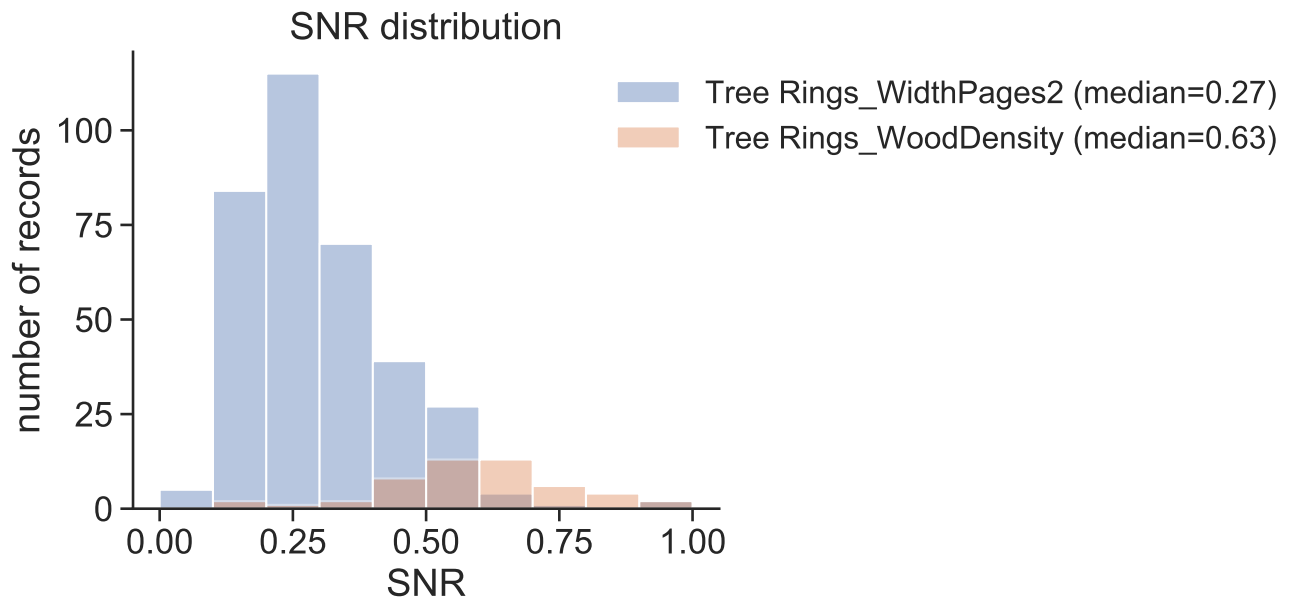
Figure S6. The signal-to-noise ratio (SNR) in TRW (Tree Rings_WidthPages2) and MXD (Tree Rings_WoodDensity) records detected by the forward operator calibration procedure (see Text S1 for details) that follows (Tardif et al., 2019) in LMR, with curated pre-defined seasonal windows. Higher SNR indicates more fraction of signal can be explained by seasonal temperature and moisture via bivariate and univariate linear regression.
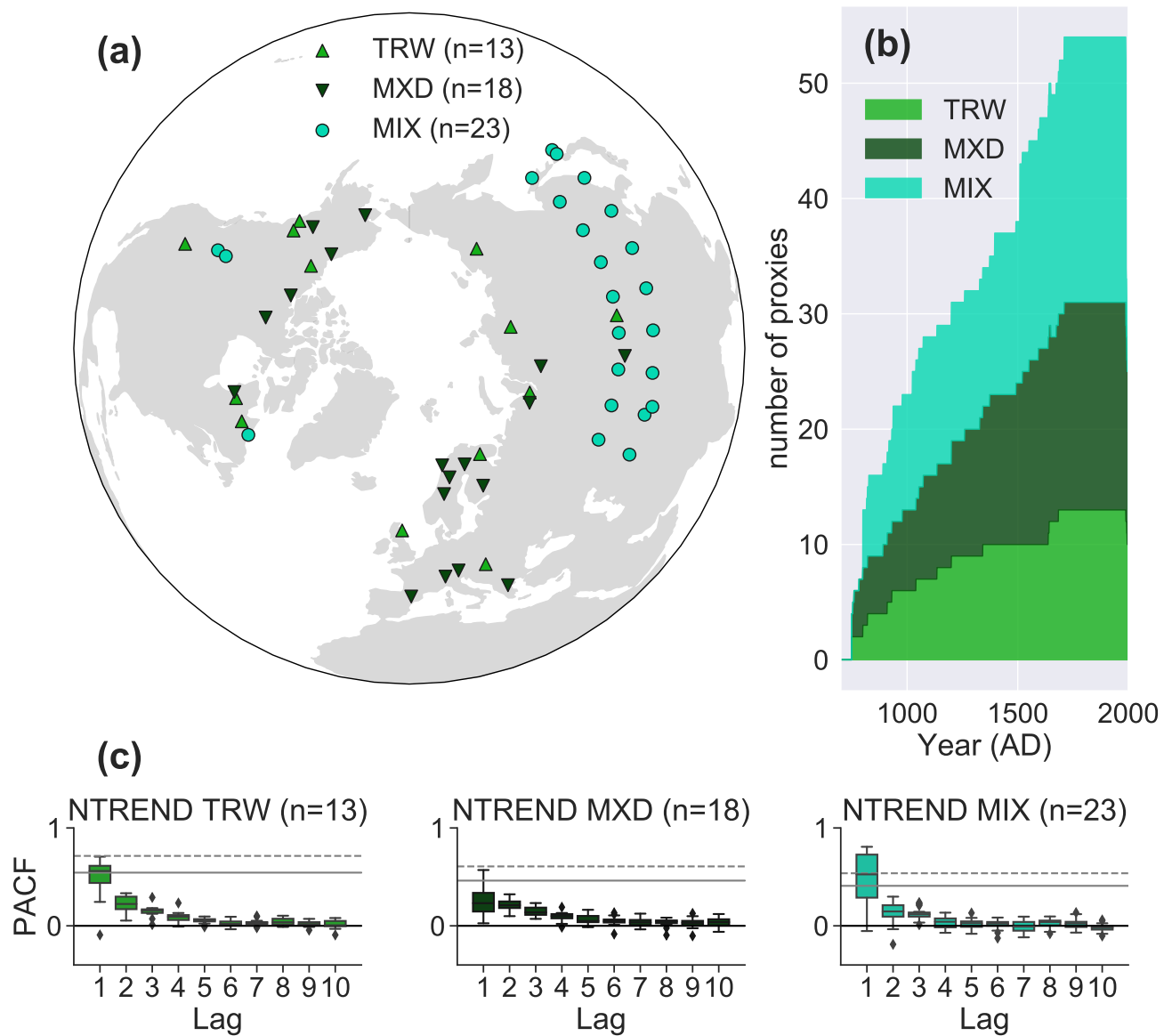
Figure S7. The Northern Hemisphere Tree-Ring Network Development (NTREND) (Wilson et al., 2016; Anchukaitis et al., 2017). (a) The spatial coverage of each proxy type. (b) The temporal availability of each proxy type. (c) The partial autocorrelation function (PACF) up to lag-10 for each proxy type.
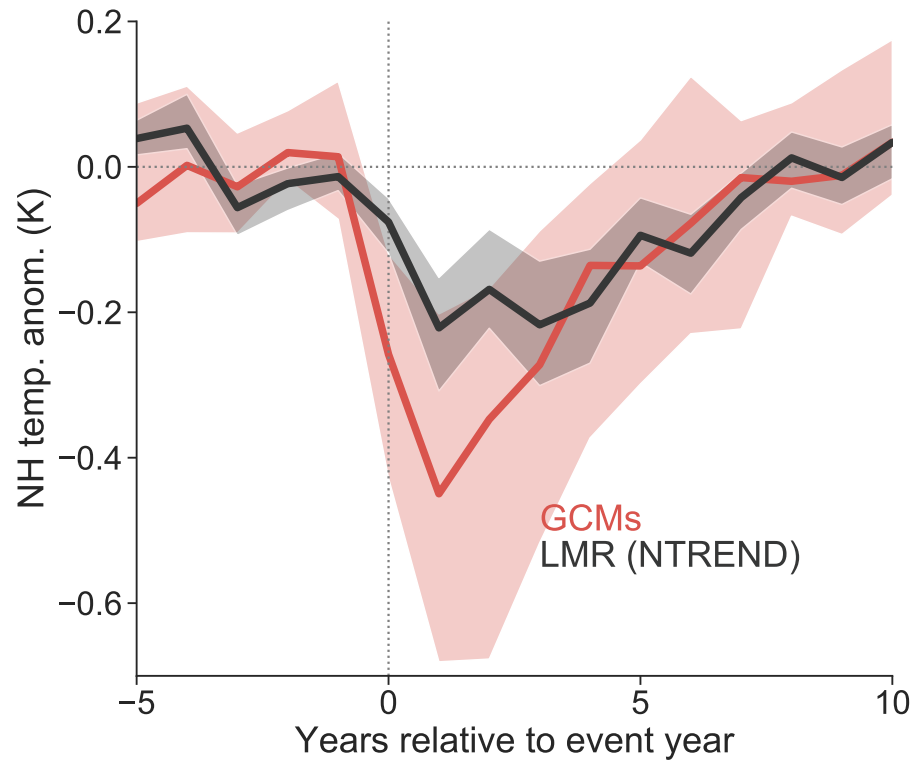
Figure S8. The comparison between the model simulated temperature response and the LMR reconstruction assimilating the whole NTREND network. SEA applied on the annual NHMT over the whole NH.
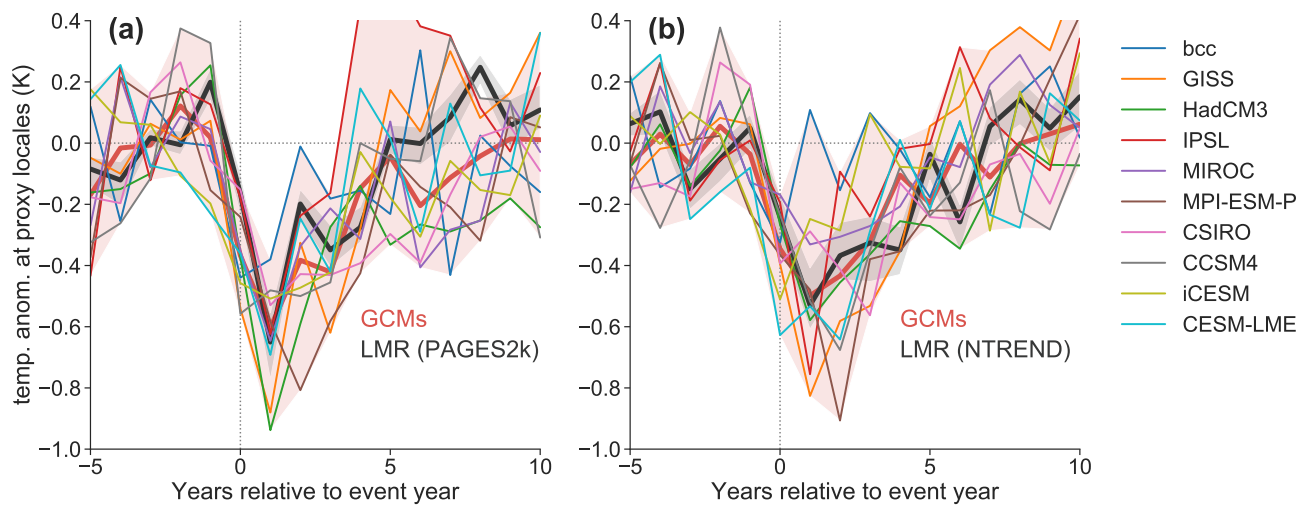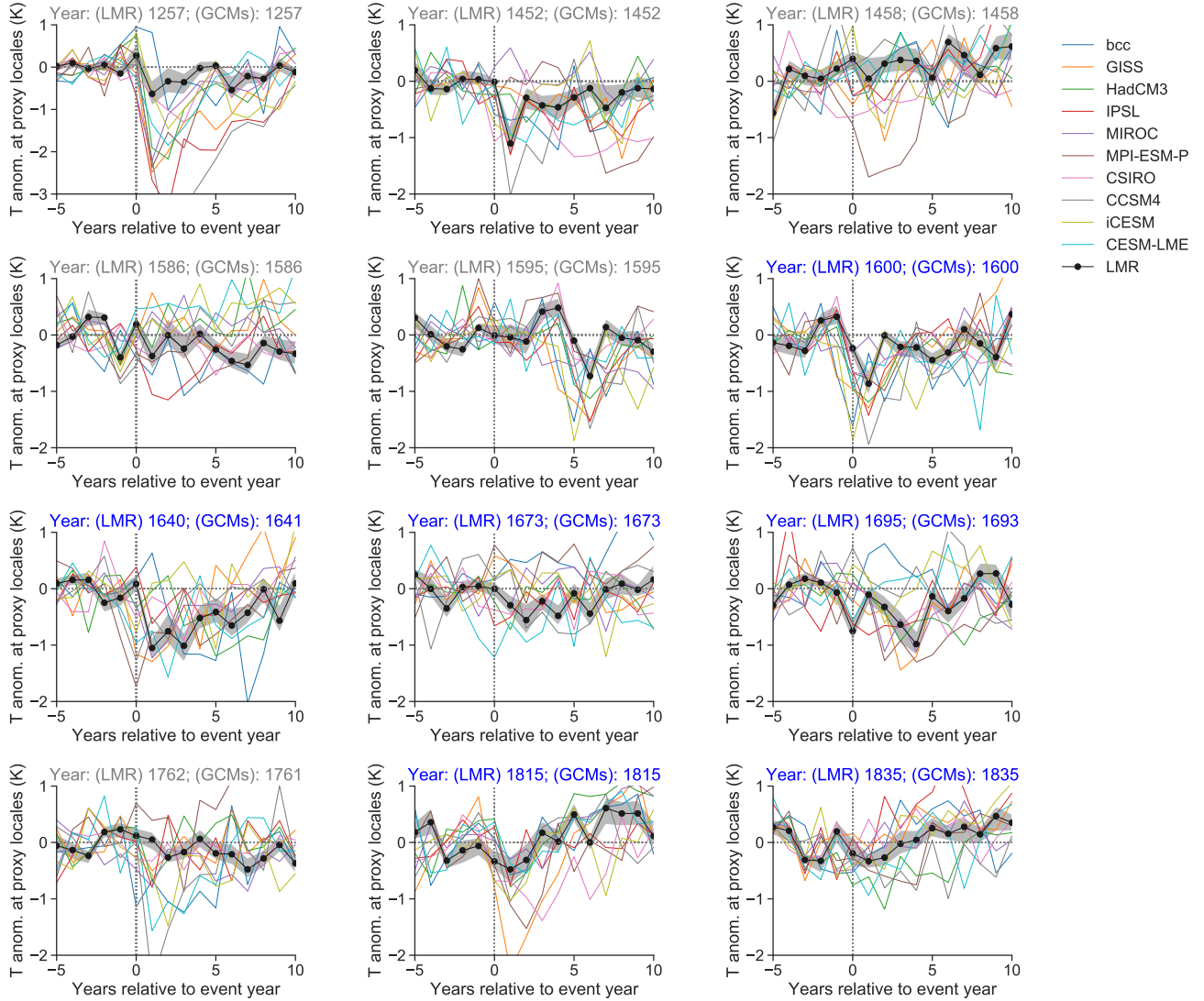

Figure S9. Similar to Fig. 4 (main text), but with the result of each model simulation plotted out.
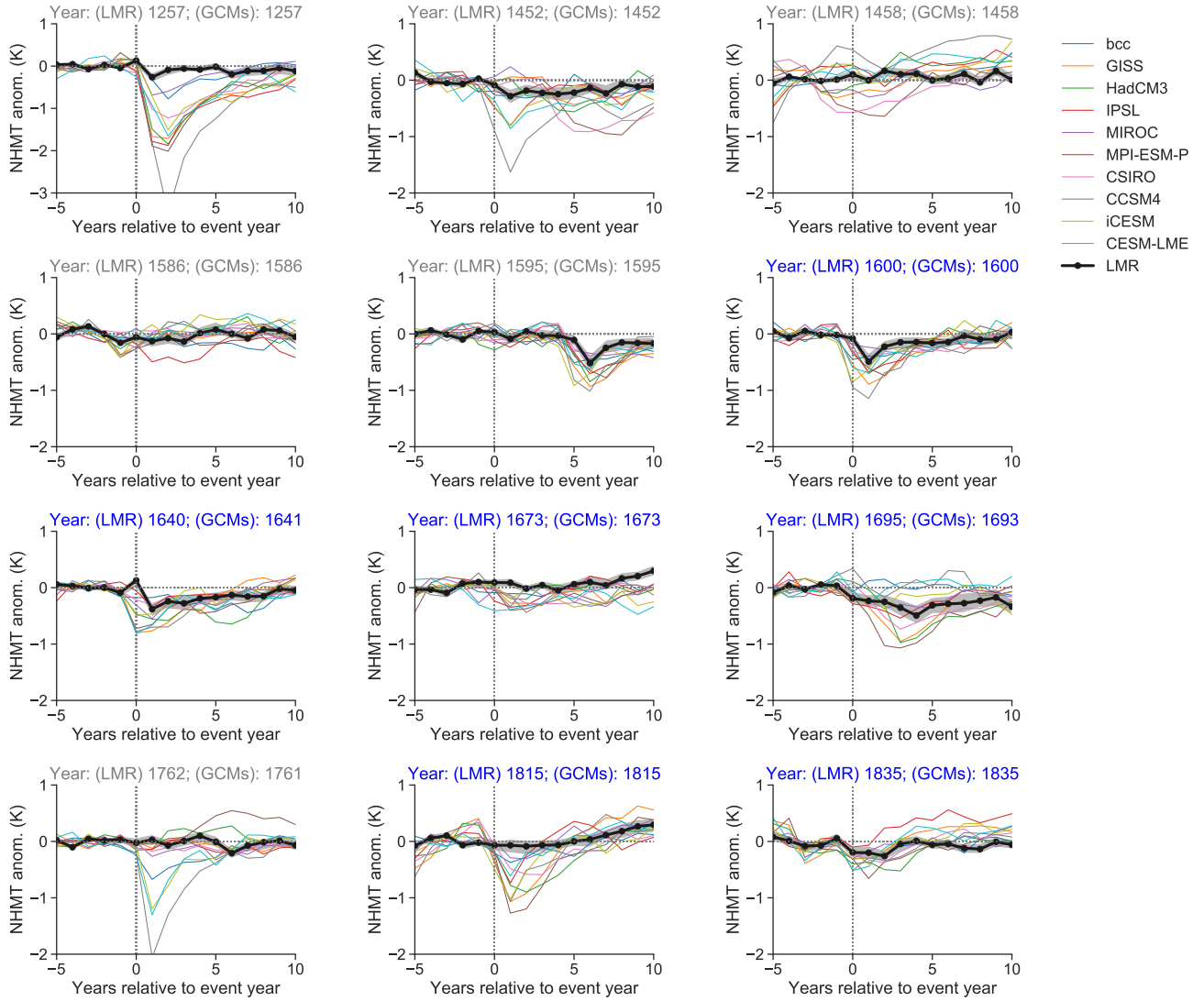
Figure S10. The temperature response to individual eruptions in LMR reconstructions assimilating the whole PAGES 2k Network and GCM simulations, targeting NHMT. The blue title denotes the 6 eruption events that are selected for SEA in our study.
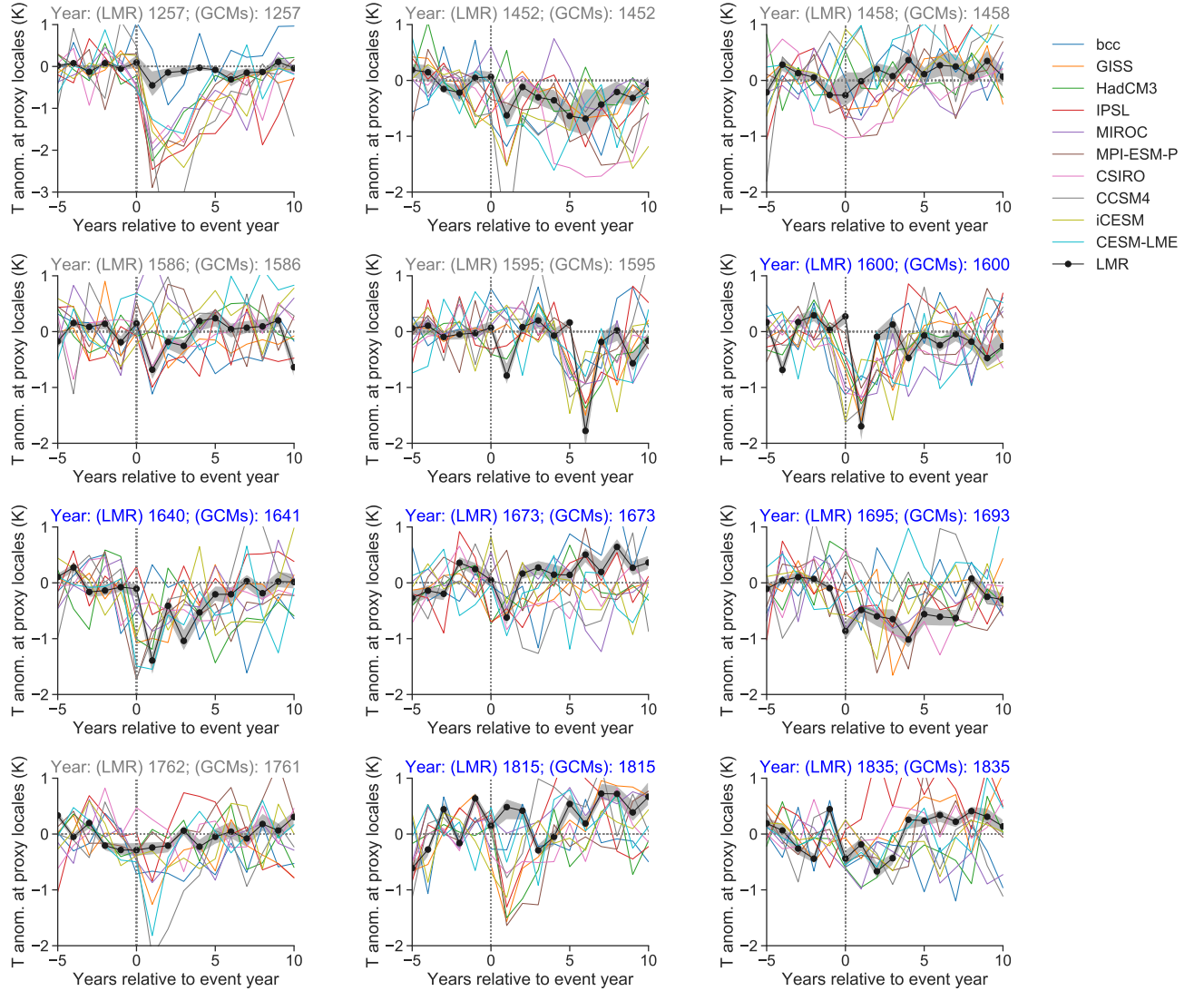
Figure S11. The temperature response to individual eruptions in LMR reconstructions assimilating the PAGES 2k MXD Network and GCM simulations, targeting mean summer temperature at proxy locales. The blue title denotes the 6 eruption events that are selected for SEA in our study.

Figure S12. The temperature response to individual eruptions in LMR reconstructions assimilating the NTREND MXD Network and GCM simulations, targeting mean summer temperature at proxy locales. The blue title denotes the 6 eruption events that are selected for SEA in our study.
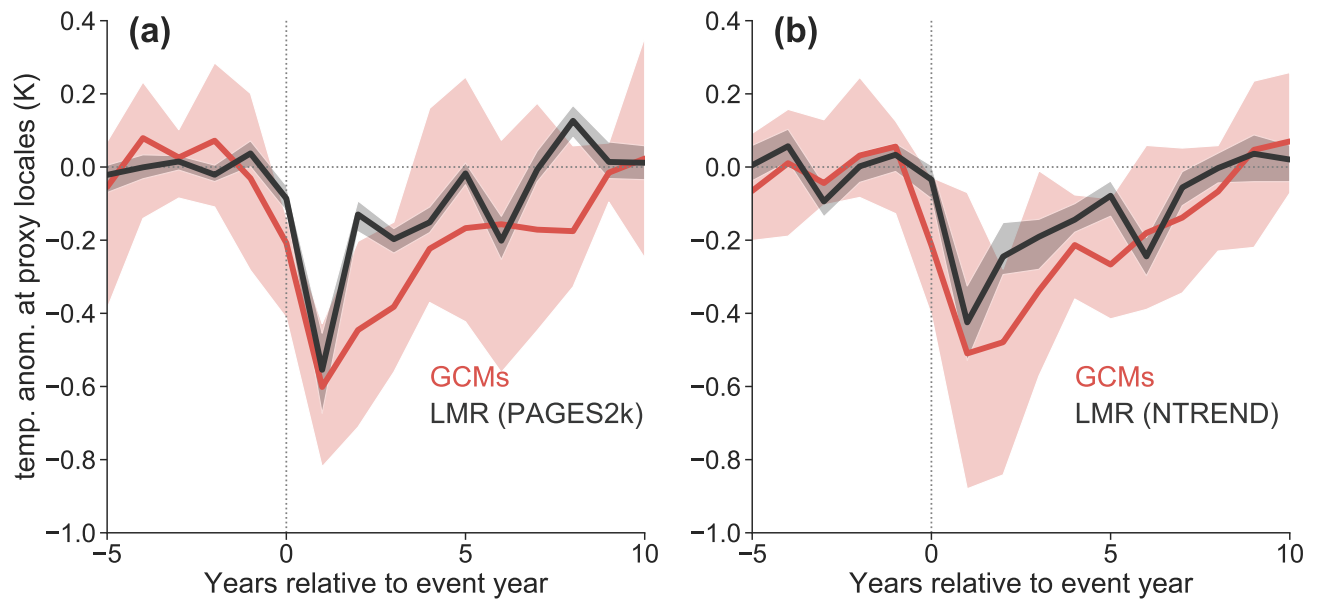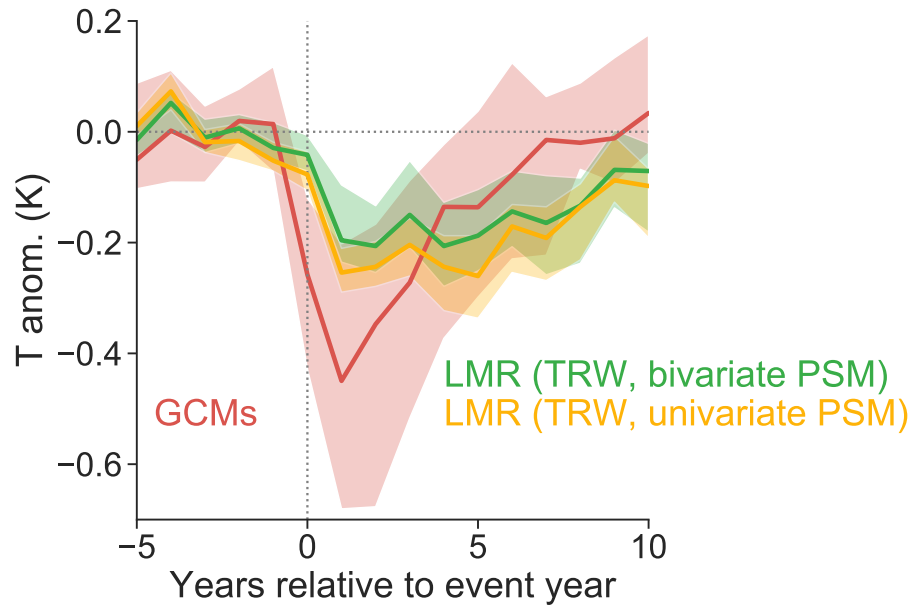
Figure S13. Same as Fig. 4 (main text), but SEA takes all eruption events listed in Fig. S10.
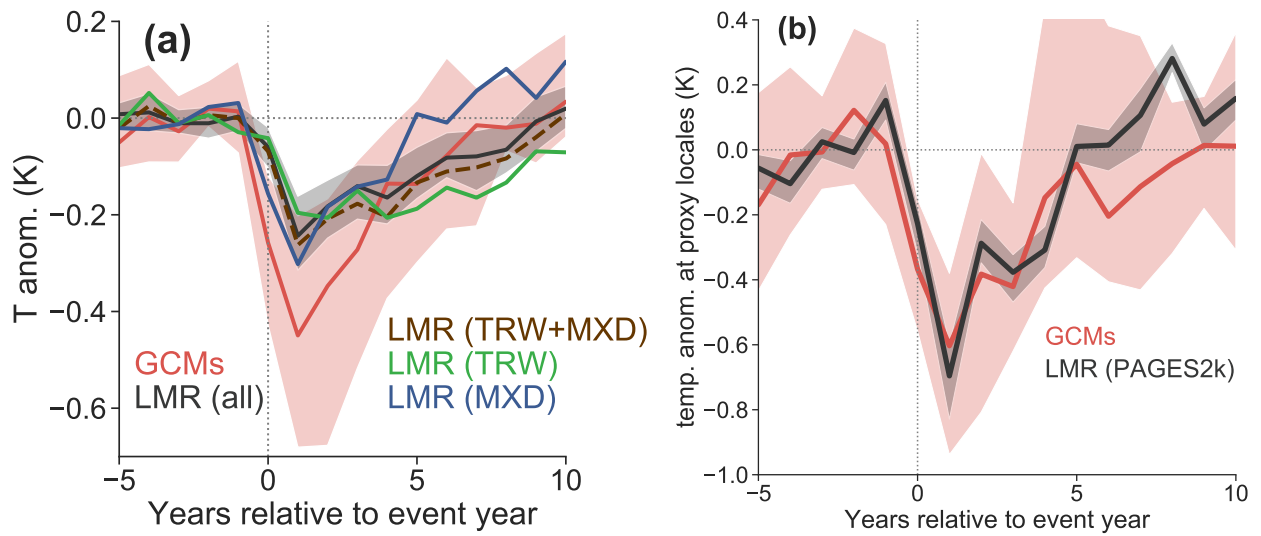
Figure S14. (a) Same as Fig. 1c (main text), but using CCSM4 as prior. (b) Same as Fig. 4a (main text), but using CCSM4 as prior.

Figure S15. Same as Fig. 1c (main text), but using CCSM4 as prior and only showing the reconstructions assimilating the PAGES2k TRW network, with both bivariate and univariate forward operator calibration. The comparison indicates that moisture information does not alleviate the issue of lagged response to volcanism in TRW records.
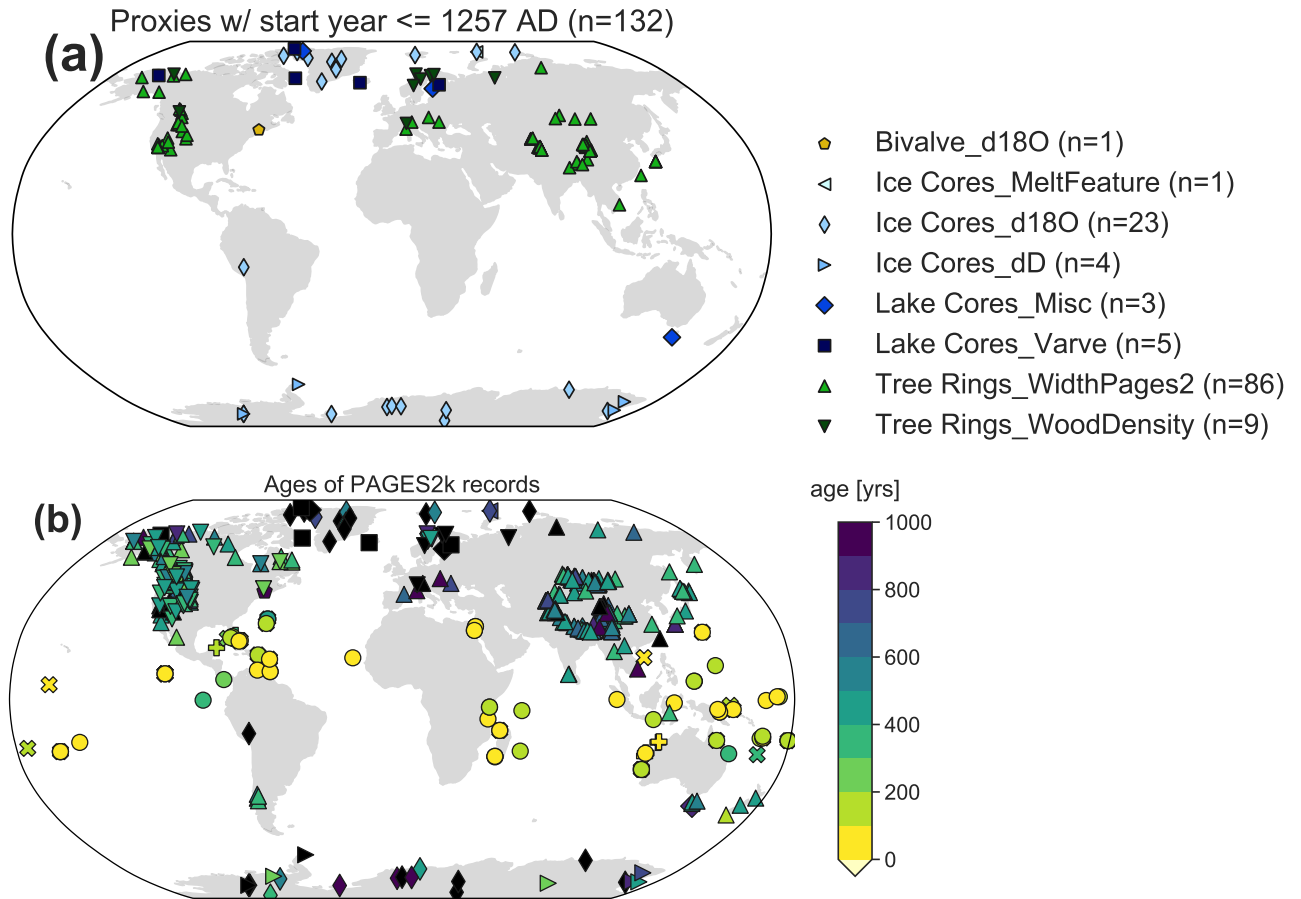
Figure S16. (a) Same as Fig. S1a, but for proxies with start year older than or equal to 1257 AD. The shapes and colors denote each proxy type. (b) Ages of PAGES2k records. The shape is same as in (a), while the colors denote different ranges of age.